Check for updates

Mantle conductivity structure beneath eastern China using 3-D geomagnetic depth sounding

Xinpeng Ma[1†], Jingru Li[2]*[†] and Kaijun Xu[1]

[1]School of Geoscience, China University of Petroleum (East China), Qingdao, China, [2]Shandong Earthquake Agency, Jinan, China

The distribution of water in the mantle plays a critical role in deep earth dynamic processes, including plate subduction, earthquake generation, and magmatic activity. Seismic tomography studies have consistently shown that the subducted Pacific plate beneath eastern China stagnates within the mantle transition zone. The release of water from the slab can substantially modify the surrounding electrical properties, producing pronounced high-conductivity anomalies. Resolving the regional conductivity structure is therefore essential for constraining the geometry and dehydration state of the stagnant slab, as well as for improving our understanding of the strong seismicity and widespread Cenozoic volcanism in eastern China. Conventional magnetotelluric (MT) surveys are constrained by their frequency range and cannot resolve deep structures on thousand-kilometer scales. Geomagnetic depth sounding (GDS), which utilizes ultra-long-period signals (>100 days), can image the mantle down to ~1,600 km, making it a powerful approach for investigating mantle water content and partial melting. Here, we compile long-term geomagnetic records from an array covering eastern China and apply a three-dimensional unstructured finite-element GDS modeling and inversion scheme. The inversion employs a limited-memory quasi-Newton optimization strategy to improve computational efficiency and model stability. The resulting electrical resistivity model delineates the mantle transition zone and lower mantle beneath eastern China, clearly imaging the stagnant Pacific slab and indicating possible dehydration and melting processes. These findings offer new constraints and insights into the structure and dynamics of the deep earth.

KEYWORDS

electrical conductivity, north China, geomagnetic depth sounding, three-dimensional inversion, mantle transition zone

1 Introduction

Eastern China has long been located at the leading edge of Pacific plate subduction, where its deep structural evolution is closely linked to regional geodynamic processes (Wu et al., 2005; Li et al., 2020; Li et al., 2021). Numerous studies have shown that volatile components—particularly water—carried by the subducting slab during its passage through the mantle transition zone (410–660 km) can substantially influence the physical properties and dynamic behavior of mantle materials (Karato, 1990; Karato, 2011; Xu et al., 2012). Water not only reduces mantle viscosity and solidus temperature, promoting partial melting, but also significantly enhances

electrical conductivity (Yoshino et al., 2008). Therefore, imaging the deep mantle's electrical structure is crucial for characterizing the distribution of hydrated mantle, identifying zones of partial melting, and understanding regional geodynamic processes (Ma et al., 2024; Lai et al., 2025).

While seismic tomography has achieved significant progress in delineating mantle structures and has revealed possible stagnant slab segments and their distribution beneath eastern China (Si et al., 2016; Lai et al., 2019), seismic velocity anomalies alone cannot directly constrain the hydration state or electrical properties of subsurface materials. To better resolve hydrated anomalies and physical property variations in the deep mantle, it is essential to employ geophysical techniques with higher sensitivity to electrical conductivity. Geomagnetic depth sounding (GDS), a passive-source electromagnetic method, analyzes long-period geomagnetic field variations at the Earth's surface to image mantle conductivity structures to depths of thousands of kilometers, offering unique advantages in revealing mantle hydration, partial melt distribution, and thermal structure (Utada et al., 2003; Kelbert et al., 2009; Kuvshinov and Semenov, 2012; Püthe et al., 2015).

However, due to limitations in data availability and computational resources, most global-scale GDS studies have focused on large-scale conductivity anomalies, resulting in low-resolution images that cannot meet the requirements for detailed structural characterization in specific regions (Kelbert et al., 2009; Semenov and Kuvshinov, 2012). Kelbert et al. (2008) emphasized that station density is a key factor limiting GDS inversion resolution. In recent years, Zhang et al. (2020) systematically compiled decades of geomagnetic observations across China and developed a stable method for extracting long-period transfer functions, thereby providing a robust data foundation for high-resolution GDS investigations.

Numerous seismic tomography studies have demonstrated that the Pacific plate has subducted into the mantle transition zone beneath eastern China, extending horizontally beneath the North China and southern Northeast China regions and forming a large mantle wedge above the stagnant slab (Huang and Zhao, 2006; Tian et al., 2016; Ma et al., 2017). Complementary to these seismic observations, Guang-Jing et al. (2015) converted geomagnetic observatory records in North China into magnetotelluric scalar impedance data, and their one-dimensional inversion revealed significant electrical contrasts across the North–South Gravity Lineament. Due to the sparse distribution of geomagnetic observatories, many subsequent studies have also relied on one-dimensional inversions of geomagnetic data to investigate this region (Egbert and Booker, 1992; Utada et al., 2003; Munch et al., 2017). However, the strong heterogeneity of mantle conductivity makes one-dimensional approaches insufficient for accurately resolving the geometry and continuity of anomalous structures. Such simplified methods fail to capture the spatial complexity necessary for regional-to large-scale deep Earth imaging. Consequently, higher-dimensional inversion techniques, particularly 3D MT modeling, are essential for providing a more reliable characterization of mantle conductivity and for advancing our understanding of subduction-related geodynamic processes in eastern China.

Against this background, the present study leverages the extensive geomagnetic network across mainland China, applying a three-dimensional unstructured tetrahedral finite-element forward modeling approach combined with a limited-memory quasi-Newton optimization scheme to investigate the deep mantle conductivity beneath eastern China (Ma et al., 2024). Using high-precision 3-D GDS imaging, we resolve the electrical structure of the mantle transition zone and the uppermost lower mantle, thereby exploring the spatial distribution of hydration and partial melting. Our results are expected to provide new geophysical evidence and theoretical constraints on the distribution of deep mantle materials and the geodynamic evolution of eastern China.

2 Data and methods

2.1 Data

To investigate the deep mantle conductivity beneath eastern China, we utilized long-term geomagnetic observations from the National Geomagnetic Network Center of China, which operates approximately 200 observatories across the country. Since 2008, a large number of newly established stations have recorded only relative geomagnetic field variations, resulting in shorter observation spans. For these stations, the maximum stable period of the derived C-response is limited to 42.7 days. In contrast, stations with more than 10 years of continuous data acquisition provide C-responses with maximum periods of up to 113.7 days (Table 1). Following a rigorous data screening process, the distribution of observatories yielding stable C-responses is shown in Figure 1.

2.2 Geomagnetic response

In GDS studies, time-series magnetic field data recorded at geomagnetic observatories are typically transformed into frequency-domain C-responses or other transfer functions to remove the influence of the source current strength. In this study, we employ the widely used C-response function. Since the variable currents in the magnetosphere can be expressed by $P_1^0(\cos\theta)$, the C-response can be written as Equation 1 (Banks, 1969):

$$C(\omega) = -\frac{a_0 \tan\theta}{2} \frac{Z}{H} = -\frac{a_0 \tan\theta}{2} \frac{H_r}{H_\theta} \qquad (1)$$

The computed C-response has units of kilometers. Under the assumption of a one-dimensional Earth and a P_1^0 source field, $\tan\theta$ can be regarded as a compensation term for the spatial structure of the source, in which case the C-response remains identical at any location on the Earth's surface.

2.3 3-D forward modeling

For a time-harmonic factor $e^{i\omega t}$, the governing curl–curl equation for the electric field in the frequency domain is Equation 2:

$$\nabla \times \nabla \times \mathbf{E} + i\omega\mu\sigma\mathbf{E} = 0 \qquad (2)$$

TABLE 1 Station details are used in this article.

Code	Longitude	Latitude	Data length	Code	Longitude	Latitude	Data length
ANQ	36.4	119.2	2007–2017	HZH	33	106.9	2007–2017
BJI	40	116.2	1957–2015	JIH	38.9	116.9	1995–2017
CDP	31	103.7	199–2017	JIN	36.6	117	2007–2017
CHL	39.7	119.2	1985–2007	LIF	36.1	111.4	2007–2017
CNH	43.8	125.3	1980–2015	LZH	36	103.9	1980–2012
DAL	38.9	121.6	1979–2007	MZL	49.6	117.4	1995–2015
DAT	40.1	113.2	2008–2017	NAJ	32	118.8	1995–2015
DED	48.5	126.2	995–2017	SHD	38.8	101	2008–2017
DFE	33.2	120.5	2011–2017	SUY	31.4	119.4	2010–2017
DIX	38.4	113	2007–2017	THE	45.2	128.2	2007–2017
DSH	38	117.7	2007–2017	WHN	30.5	114.6	1995–2007
FEN	41.2	116.6	2008–2017	XLH	43.9	116.1	2008–2017
GUP	36.5	115	2007–2017	YIK	40.7	122.6	2008–2017
HAA	32.5	120.5	2008–2017	YLN	38.4	109.7	2009–2017
HAB	45.7	126.4	2008–2017	ZHW	37.6	105.2	2007–2017
HAZ	30.2	120.2	1960–2007				

where ω is the angular frequency, μ_0 is the magnetic permeability of free space, σ is the electrical conductivity, and $\mathbf{E}$ denote the electric field intensities.

The forward modeling is implemented using the finite element method (FEM). Within each tetrahedral element, the electric field is expressed as Equation 3:

$$\tilde{\mathbf{E}} = \sum_{j=1}^{ndof} E_j \mathbf{N}_j \qquad (3)$$

where $\mathbf{N}_j$ is the vector interpolation basis function, and E_j is the electric field value at the midpoint of the element edge.

Applying the Galerkin method yields Equation 4:

$$(\mathbf{A} + i\omega\mu\mathbf{M})\mathbf{E} = i\omega\mathbf{S} \qquad (4)$$

where $\mathbf{A}$ and $\mathbf{M}$ are the stiffness and mass matrices of the tetrahedral element, respectively, and $\mathbf{S}$ is the source term on the outer boundary. The specific expressions are Equations 5–7:

$$\mathbf{A} = \iint_{\Omega} (\nabla \times \mathbf{N}) \cdot (\nabla \times \mathbf{N}) d\Omega \qquad (5)$$

$$\mathbf{M} = \iint_{\Omega} \mathbf{N} \cdot \sigma \cdot \mathbf{N} d\Omega \qquad (6)$$

$$\mathbf{S} = \iint_{\Gamma} \mathbf{N} \cdot (\boldsymbol{n} \times \mathbf{B}_0) d\Gamma \qquad (7)$$

The external magnetic field is given by Equation 8:

$$\begin{cases} \mathbf{B}_r^e = -\varepsilon_1^0 \cos\theta \\ \mathbf{B}_\theta^e = \varepsilon_1^0 \sin\theta \\ \mathbf{B}_\varphi^e = 0 \end{cases} \qquad (8)$$

2.4 Inversion theory

The 3-D inversion problem for GDS can be formulated as finding the optimal model $\mathbf{m}$ that minimizes the objective function, as shown in Equation 9:
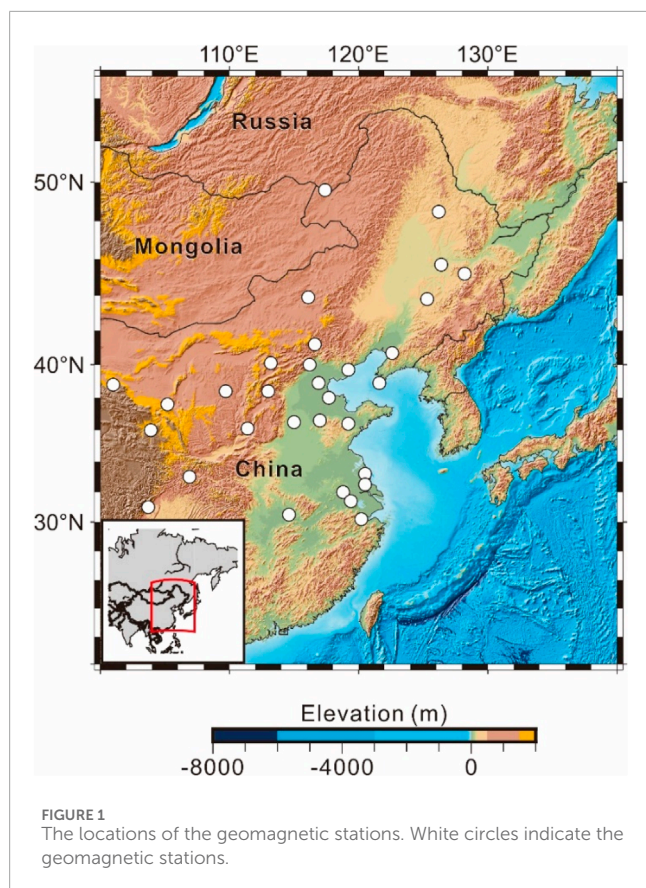
$$\Phi(\mathbf{m}, \lambda) = \Phi_d(\mathbf{m}) + \lambda\Phi_m(\mathbf{m}) \qquad (9)$$

Here, $\Phi_d(\mathbf{m})$ and $\Phi_m(\mathbf{m})$ represent the data misfit term and the model regularization term, respectively, and λ is the regularization parameter that balances their relative contributions.

In this study, the objective function is defined using the L2 norm minimizes the objective function, as shown in Equation 10:

$$\Phi(\mathbf{m}, \lambda) = \left\| \mathbf{C}_d^{-1/2}(\psi(\mathbf{m}) - \mathbf{d}) \right\|_2^2 + \lambda \left\| \mathbf{C}_m^{-1/2}(\mathbf{m} - \mathbf{m}_0) \right\|_2^2 \qquad (10)$$

where $\mathbf{d}$ is the observed data vector, m and m_0 are the model and initial model parameter vectors, respectively. $\psi(\mathbf{m})$ is the forward

The locations of the geomagnetic stations. White circles indicate the geomagnetic stations.

1. Initialize the regularization parameter λ and the initial Hessian matrix H_i;

2. Set the iteration counter $i = 1$ and select an initial model m_i, define the data misfit threshold $\varepsilon = 1.0$;

3. While $\eta \leq \varepsilon$ or η does not decrease significantly Do

4. Conduct forward modeling.

5. Compute the data misfit η and the gradient of the objective function $\mathbf{g}_i = -\nabla\varphi(\mathbf{m}_i, \mathbf{d})$;

6. Set $\mathbf{u}_i = \mathbf{H}_i \mathbf{g}_i$, and determine an appropriate step length α_i to update the model $\mathbf{m}_{i+1} = \mathbf{m}_i + \alpha_i \mathbf{u}_i$;

7. Perform forward and adjoint forward modeling to compute the new gradient.

8. IF η does not decrease significantly compared with the previous iteration THEN

9. Reduce the regularization parameter λ;

10. END IF

11. Update the Hessian matrix: $\mathbf{H}_{i+1} = \left(\mathbf{I} - \rho_i \mathbf{s}_i \mathbf{y}_i^T\right)\mathbf{H}_i\left(\mathbf{I} - \rho_i \mathbf{y}_i \mathbf{s}_i^T\right) + \rho_i \mathbf{s}_i \mathbf{s}_i^T$; where $\rho_i = 1/\left(\mathbf{y}_i^T \mathbf{s}_i\right), \mathbf{s}_i = \mathbf{m}_{i+1} - \mathbf{m}_i, \mathbf{y}_i = \nabla\varphi(\mathbf{m}_{i+1}, \mathbf{d}) - \nabla\varphi(\mathbf{m}_i, \mathbf{d})$;

12. Increment the iteration counter: $i = i + 1$

13. END While

14. Output the final model m_i.

response of the model, and $\mathbf{C}_d^{-1/2}$ and $\mathbf{C}_m^{-1/2}$ are the covariance operators for the data and the model.

The inversion is performed using the limited-memory Broyden–Fletcher–Goldfarb–Shanno (L-BFGS) algorithm, which introduces a limited-memory strategy into the classical BFGS optimization method. This modification significantly reduces memory requirements and addresses efficiency issues caused by the loss of the inverse Hessian matrix during the initial

The map of global surface conductance.
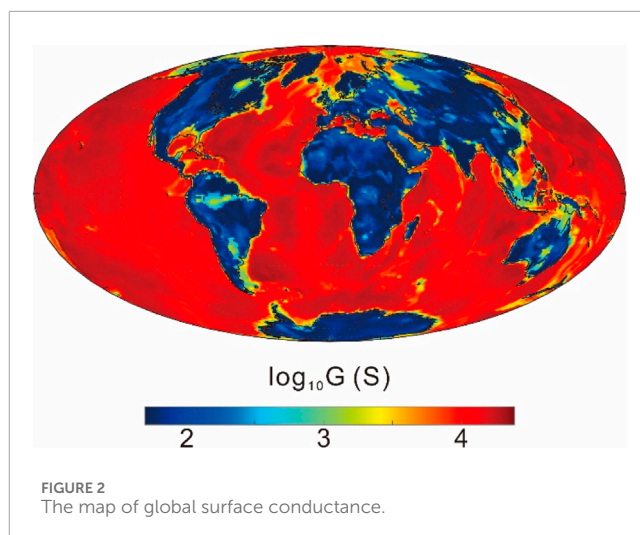
iterations, making L-BFGS particularly suitable for large-scale 3-D electromagnetic inversion problems.

The L-BFGS workflow applied in this study is as follows:

3 Results

A pronounced contrast in conductivity between land and ocean produces the so-called ocean induction effect, which introduces significant distortions in C-response data. Kuvshinov et al. (2002) demonstrated that such effects strongly influence the responses of coastal geomagnetic stations, particularly within a period range of up to ~20 days. It is therefore essential to account for ocean induction effects in three-dimensional GDS inversion. A common approach is to approximate Earth's surface conductivity using a 10° × 10° land–ocean grid, however, this simplification can still result in considerable errors. To overcome this limitation, Ma et al. (2024) proposed a novel three-dimensional GDS inversion method that directly incorporates the real Earth surface conductivity distribution into the inversion model. Following this strategy, we also adopt the actual surface conductivity distribution in our inversion, as shown in Figure 2 (Everett et al., 2003).
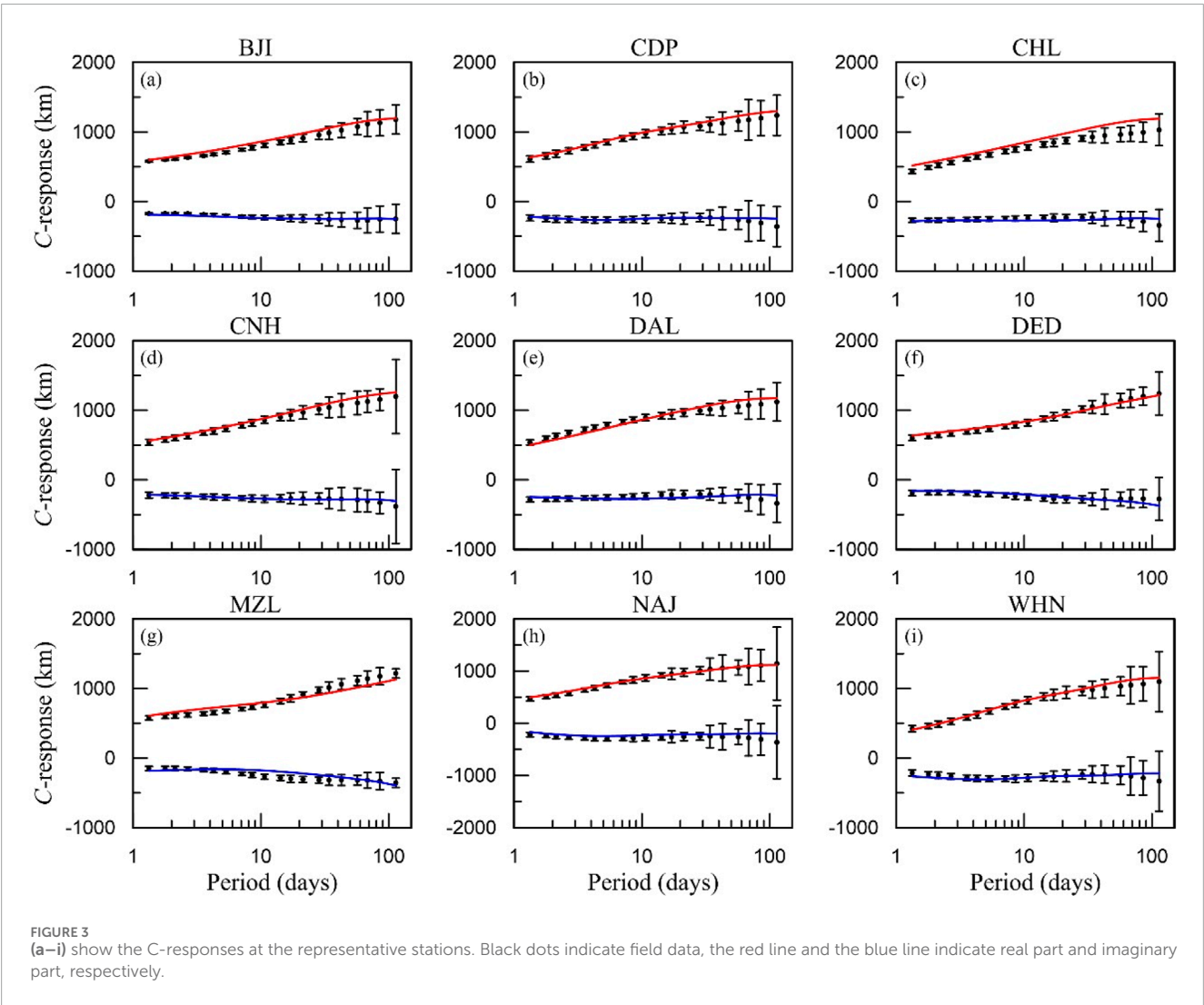
The inversion was initialized using the global mean conductivity model of Kelbert et al. (2009) as the background (Table 2). In this setup, the eight layers above 1,600 km depth were allowed to vary freely, whereas the four layers between 1,600 km and the outer core were fixed and laterally homogeneous, owing to the limited sensitivity of geomagnetic induction to conductivity structure at such depths. The model was discretized into an unstructured tetrahedral mesh with 943,513 elements. The regularization parameter was initially set to $\lambda = 100$ and updated iteratively using a cooling strategy (Zhdanov, 2002).

Observed and modeled responses for representative stations are shown in Figure 3. Short-period responses are well reproduced, whereas slight misfits appear at the longest periods for a few stations, likely due to the limited availability and lower reliability of long-period observations. Within the period range used in this study, these discrepancies exert minimal influence on conductivity estimates at depths greater than ~1,000 km.

TABLE 2 One-dimensional layered earth resistivity model.

Layer	Depth (km)	Res. (Ω·m)	Layer	Depth (km)	Res. (Ω·m)
1	0–50	Real	2	50–100	157
3	100–250	100	4	250–410	20
5	410–520	10	6	520–670	3.16
7	670–900	1	8	900–1200	1
9	1200–1600	1	10	1600–2000	1
11	2000–2400	0.316	12	2400–2890	0.1
13	2890–6371	0.00001			

FIGURE 3
(a–i) show the C-responses at the representative stations. Black dots indicate field data, the red line and the blue line indicate real part and imaginary part, respectively.

To highlight deviations from the background model, the inverted three-dimensional conductivity structure was compared with the one-dimensional background model (Table 2). We computed the logarithmic ratio between the two and plotted horizontal slices for the region 10°–60°N, 90°–140°E (Figure 4). Given the shortest period used (1.13 days), the model is insensitive to structures shallower than ~200 km. Considering the optimal resolving capability of GDS for depths between 410
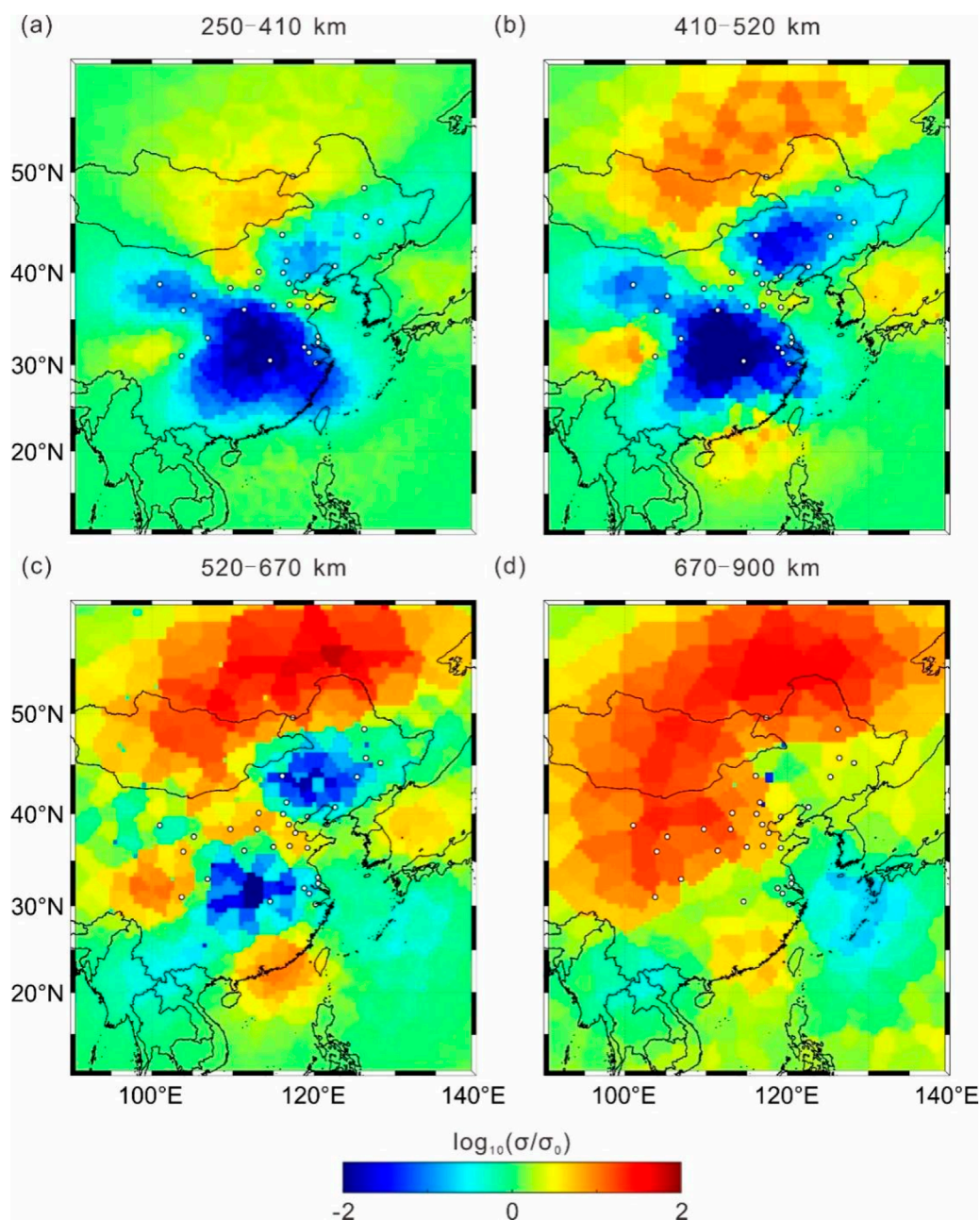
FIGURE 4
Electrical conductivity model of the mantle beneath eastern China, where Figure 3 (a–d) represent the models at different depths.

and 1,200 km (Kelbert et al., 2009), we mainly present results for depths of 250–900 km. Interpretation focuses on mainland China and adjacent offshore regions where station coverage is adequate, and large-scale anomalies in Mongolia and Russia, where no station control exists, are not discussed.

At depths of 250–410 km, two pronounced high-resistivity anomalies occur in central China and central–northeastern China, while the Shandong Peninsula and Bohai Bay periphery exhibit high conductivity. Between 410 and 520 km depth, the high-resistivity anomaly in northeastern China intensifies, and a high-conductivity anomaly emerges in the South China–South China

Sea region, spatially coinciding with the Hainan mantle plume location identified by Li and Liu (2023). This conductor extends upward from the lower mantle through the transition zone into the upper mantle.

Between 520 and 670 km depth, the Bohai Bay conductor extends westward and develops a north–south trend. This anomaly may be related to the water-rich stagnant slab from the western Pacific subduction in northeastern China and matches the low-velocity structure beneath the Yanshan Orogen in seismic tomography images. During the same depth range, the high-resistivity anomaly in central China decreases in extent.

In the 670–900 km depth range, the previously observed high-resistivity anomalies become less distinct, and high conductivity dominates in the North China and Inner Mongolia regions, possibly reflecting the deep thermo-mechanical structure beneath the North–South Seismic Belt. In the western segment of the Central Orogenic Belt, conductivity gradients with depth remain relatively uniform and markedly lower than in surrounding regions, suggesting the presence of a relatively cold mantle channel, whose potential connection with a deep cold plume warrants further investigation.

Overall, the mantle electrical structure beneath eastern China is characterized by: (1) significant high-resistivity anomalies in central–northeastern China and central China between 250 and 670 km; (2) a persistent high-conductivity anomaly beneath the South China Sea–Hainan region from 410 to 900 km, potentially linked to mantle plume activity; and (3) a high-conductivity belt beneath the Bohai Bay and surrounding areas between 520 and 900 km, extending westward and along a north–south axis, likely influenced by the stagnant slab and its hydration. These conductivity patterns are consistent with seismic velocity structures and lithospheric geodynamic evidence.

4 Conclusion

This study presents, for the first time, a three-dimensional electrical conductivity model of the mantle beneath eastern China derived from C-response data spanning periods of 3.5–113 days, obtained from regional geomagnetic observatories. The inversion results reveal a vertically continuous conductive anomaly between 250 and 900 km depth, centered beneath the Shandong Peninsula and Bohai Bay. The conductivity model supports the interpretation that the western Pacific subduction zone delivers significant amounts of water into the mantle transition zone and provides strong evidence for the existence of the Hainan plume.

It should be noted, however, that the depth sensitivity of GDS limits its ability to resolve the geometry of stagnant slabs in the shallow upper mantle. Complementary approaches, such as long-period MT, can be employed to better constrain the upper mantle conductivity structure. Future research integrating GDS and long-period MT data through joint inversion is expected to significantly enhance our capability to investigate subduction zone processes.

Data availability statement

The data used for inversion can be downloaded from the World Data Centre. The original contributions presented in the study are included in the article, further inquiries can be directed to the corresponding author.

Author contributions

XM: Writing – original draft, Writing – review and editing, Conceptualization, Methodology, Software, Visualization, Supervision. JL: Conceptualization, Data curation, Funding acquisition, Visualization, Writing – original draft, Writing – review and editing. KX: Formal Analysis, Funding acquisition, Project administration, Supervision, Writing – review and editing.

Funding

Conflict of interest

The authors declare that the research was conducted in the absence of any commercial or financial relationships that could be construed as a potential conflict of interest.

The handling editor BZ declared a past co-authorship with one of the authors XM.

Generative AI statement

The author(s) declare that no Generative AI was used in the creation of this manuscript.

Any alternative text (alt text) provided alongside figures in this article has been generated by Frontiers with the support of artificial intelligence and reasonable efforts have been made to ensure accuracy, including review by the authors wherever possible. If you identify any issues, please contact us.

Publisher's note

References

Banks, R. J. (1969). Geomagnetic variations and the electrical conductivity of the upper mantle. *Geophys. J. Int.* 17 (5), 457–487. doi:10.1111/j.1365-246X.1969.tb00252.x

Egbert, G. D., and Booker, J. R. (1992). Very long period magnetotellurics at Tucson Observatory—Implications for mantle conductivity. *J. Geophys. Res.* 97 (B11), 15 099–15 112. doi:10.1029/92jb01251

Everett, M. E., Constable, S., and Constable, C. G. (2003). Effects of near-surface conductance on global satellite induction responses. *Geophys. J. Int.* 153 (1), 277–286. doi:10.1046/j.1365-246X.2003.01906.x

Guang-Jing, X. U., Ji, TANG, Huang, Q.-H., and Uyeshima, M. (2015). Study on the conductivity structure of the upper mantle and transition zone beneath north China. *Chin. J. Geophys. (in Chinese)* 58 (2), 566–575. doi:10.6038/cjg20150219

Huang, J., and Zhao, D. (2006). High-resolution mantle tomography of China and surrounding regions. *Journal of Geophysical Research* 111, B09305. doi:10.1029/2005jb004066

Karato, S. (1990). The role of hydrogen in the electrical conductivity of the upper mantle. *Nature* 347 (6290), 272–273. doi:10.1038/347272a0

Karato, S.-I. (2011). Water distribution across the mantle transition zone and its implications for global material circulation. *Earth planet. Sci. Lett.* 301, 413–423. doi:10.1016/j.epsl.2010.11.038

Kelbert, A., Egbert, G. D., and Schultz, A. (2008). Non-linear conjugate gradient inversion for global EM induction: resolution studies. *Geophysical Journal International* 173 (2), 365–381. doi:10.1111/j.1365-246X.2008.03717.x

Kelbert, A., Schultz, A., and Egbert, G. (2009). Global electromagnetic induction constraints on transition-zone water content variations. *Nature* 460 (7258), 1003–1006. doi:10.1038/nature08257

Kuvshinov, A., and Semenov, A. (2012). Global 3-D imaging of mantle electrical conductivity based on inversion of observatory C-responses-I. An approach and its verification: 3-D imaging of mantle conductivity-I. *Geophys. J. Int.* 189, 1335–1352. doi:10.1111/j.1365-246X.2011.05349.x

Kuvshinov, A. V., Olsen, N., Avdeev, D. B., and Pankratov, O. V. (2002). Electromagnetic induction in the oceans and the anomalous behaviour of coastal C-responses for periods up to 20 days. *Geophysical Research Letters* 29 (12), 36-1–4. doi:10.1029/2001gl014409

Lai, Y., Chen, L., Wang, T., and Zhan, Z. (2019). Mantle transition zone structure beneath northeast Asia from 2-D triplicated waveform modeling: implication for a segmented stagnant slab. *Journal of Geophysical Research Solid Earth* 124 (2), 1871–1888. doi:10.1029/2018JB016642

Lai, M., Ren, X., Yin, C., Liu, Y., Ma, X., Wang, Y., et al. (2025). Electrical conductivity of mantle transition zone and water content revealed by the magnetic data of China seismo-electromagnetic satellite. *IEEE Journal of Selected Topics in Applied Earth Observations and Remote Sensing* 18, 3173–3184. doi:10.1109/JSTARS.2024.3523671

Li, S., and Liu, Y. (2023). Cold and wet mantle transition zone beneath the Mediterranean Sea revealed by the electrical image. *Applied Sciences* 13 (2), 689. doi:10.3390/app13020689

Li, S., Weng, A., Zhang, Y., Schultz, A., Li, Y., Tang, Y., et al. (2020). Evidence of Bermuda hot and wet upwelling from novel three-Dimensional global mantle electrical conductivity image. *Geochemistry, Geophysics, Geosystems* 21 (6), e2020GC009016. doi:10.1029/2020GC009016

Li, Y., Weng, A., Xu, W., Zou, Z., Tang, Y., Zhou, Z., et al. (2021). Translithospheric magma plumbing system of intraplate volcanoes as revealed by electrical resistivity imaging. *Geology* 49 (11), 1337–1342. doi:10.1130/G49032.1

Ma, J., Tian, Y., Liu, C., Zhao, D., Feng, X., and Zhu, H. (2017). P-wave tomography of northeast Asia: constraints on the Western Pacific plate subduction and mantle dynamics. *Phys. Earth Planet. Inter.* doi:10.1016/j.pepi.2017.11.003

Ma, X., Liu, Y., Yin, C., Li, J., Li, J., Ren, X., et al. (2024). Global mantle conductivity imaging using 3-D geomagnetic depth sounding with real Earth surface conductivity constraint. *Computers and Geosciences* 192 (October), 105697. doi:10.1016/j.cageo.2024.105697

Munch, F. D., Grayver, A. V., Kuvshinov, A. V., and Khan, A. (2017). Stochastic inversion of geomagnetic observatory data including rigorous treatment of the ocean induction effect with implications for transition zone water content and thermal structure. *Journal of Geophysical Research Solid Earth* 123, 31–51. doi:10.1002/2017jb014691

Püthe, C., Kuvshinov, A., Khan, A., and Olsen, N. (2015). A new model of earth's radial conductivity structure derived from over 10 Yr of satellite and observatory magnetic data. *Geophysical Journal International* 203 (3), 1864–1872. doi:10.1093/gji/ggv407

Semenov, A., and Kuvshinov, A. (2012). "Global 3-D imaging of mantle conductivity based on inversion of observatory C -Responses-II. Data analysis and results: 3-D imaging of mantle Conductivity-II. *Geophysical Journal International* doi:10.1111/j.1365-246X.2012.05665.x

Si, S., Zheng, Y., Liu, B., and Tian, X. (2016). Structure of the Mantle transition Zone beneath the north China craton. *Journal of Asian Earth Sciences* 116 (February), 69–80. doi:10.1016/j.jseaes.2015.11.006

Tian, Y., Zhu, H., Zhao, D., Liu, C., Feng, X., Liu, T., et al. (2016). Mantle transition zone structure beneath the Changbai volcano: insight into deep slab dehydration and hot upwelling near the 410 km discontinuity. *Journal of Geophysical Research Solid Earth* 121, 5794–5808. doi:10.1002/2016jb012959

Utada, H., Koyama, T., Shimizu, H., and Chave, A. D. (2003). A semi-global reference model for electrical conductivity in the mid-mantle beneath the north Pacific region. *Geophysical Research Letters* 30 (4). doi:10.1029/2002GL016092

Wu, F.-Y., Lin, J.-Q., Wilde, S. A., Zhang, X. 'Ou, and Yang, J.-H. (2005). Nature and significance of the Early Cretaceous giant igneous event in eastern China. *Earth and Planetary Science Letters* 233 (1), 103–119. doi:10.1016/j.epsl.2005.02.019

Xu, Y.-G., Zhang, H.-H., Qiu, H.-N., Ge, W.-C., and Wu, F.-Y. (2012). Oceanic crust components in Continental basalts from shuangliao, northeast China: derived from the mantle transition zone? *Chemical Geology, Geochemical Perspectives on Mantle Dynamics and Plate Interactions in Asia A Special Issue in Honor/Memory of Dr. Shen-su Sun* 328 (October), 168–184. doi:10.1016/j.chemgeo.2012.01.027

Yoshino, T., Manthilake, G., Matsuzaki, T., and Katsura, T. (2008). Dry mantle transition zone inferred from the conductivity of wadsleyite and ringwoodite. *Nature* 451 (7176), 326–329. doi:10.1038/nature06427

Zhang, Y., Weng, A., Li, S., Yue, Y., Tang, Yu, and Liu, Y. (2020). Electrical conductivity in the mantle transition zone beneath eastern China derived from L1-Norm C-Responses. *Geophysical Journal International* 221 (2), 1110–1124. doi:10.1093/gji/ggaa059

Zhdanov, M. S. (2002). "Geophysical inverse theory and regularization problems," in *Methods in geochemistry and geophysics 36.* Elsevier Science.